Distributed Robust Control of Compliant Framed Wheeled Modular Mobile Robots

Xiaorui Zhu
ASME Student Member

Mark A. Minor
ASME Member
e-mail: minor@mech.utah.edu

Sungyong Park

Department of Mechanical Engineering,
University of Utah,
Salt Lake City, Utah 84112

A distributed robust controller for Compliant Framed wheeled Modular Mobile Robots (CFMMR) is studied in this paper. This type of wheeled mobile robot uses rigid axles coupled by compliant frame modules to provide both full suspension and enhanced steering capability without additional hardware. In this research, a distributed nonlinear damping controller using backstepping techniques for wheel-torque control is first developed for single-axle unicycle type robots. The controller is then extended to multiple-axle CFMMR configurations and is robust to disturbances created by modeling errors; especially highly nonlinear frame forces caused by axle interaction. In particular, the controller considers time-varying reference velocities and allows the robot to perform posture regulation, path following, or general trajectory tracking. A two-axle scout CFMMR configuration is used to evaluate the controller. Simulation and experimental results verify robust dynamic motion control of path following. [DOI: 10.1115/1.2229254]

1 Introduction

A distributed robust dynamic control algorithm for multi-axle Compliant Framed wheeled Modular Mobile Robots (CFMMR) is developed in this paper. A two-axle CFMMR, Fig. 1, is used for testing in the experiments. The CFMMR concept is unique in two ways. First, it uses a novel yet simple structure to provide suspension and highly controllable steering capability without any additional hardware. This is accomplished by compliant frame elements that couple rigid differentially steered axles. In this study, a partially compliant frame provides roll and yaw Degrees of Freedom (DOF) for suspension and steering capability, respectively. The CFMMR also improves the modularity of wheeled mobile robotics by allowing frame and axle modules to be assembled in configurations customized for specific tasks. It is argued that homogeneity reduces maintenance, offers increased robustness through redundancy, provides compact and ordered storage, and increases adaptability [1,2]. Despite these attributes, the CFMMR provides new challenges in motion control [3–5], sensor instrumentation [6], and data fusion [6].

A limited number of compliant vehicles have been investigated in the last few decades, and none possess a similar highly compliant frame whose deflection is controlled by coordinated actuation of the wheels. The earliest platform is a system proposed for planetary exploration using compliant members to provide roll and pitch DOF for suspension of the axles [7] to adapt to the terrain. More recent research has introduced compliance to accommodate measurement error and prevent wheel slip from occurring between independently controlled axle units on a service robot [8]. This robot is similar in spirit to the CFMMR in that it allows relative rotation between the axles, but this compliance is provided by rotary joints connected to the ends of a frame with limited prismatic compliance. Some snake-like robots also use wheeled body modules, but they are usually connected in series by articulated joints. Some have active joints and passive wheels [9] while others have active wheels and either partially active [10,11] or entirely passive joints [12]. Active wheels provide direct control over forward velocity and are better for traveling over terrain. Active joints allow direct control over robot shape, but they are too slow for high-speed movement. Active-wheel passive-joint snake-like robots, which are most similar to the CFMMR, are thus desirable for natural terrain adaptation and faster travel over rugged terrain [12]. Compared to the complex and expensive mechanical joints in all of these robots, the CFMMR is much simpler, and is thus less expensive and has less potential for mechanical failure.

The control of compliance in robotic systems has been predominant among flexible manipulators, where oscillations are a primary concern [13,14]. Compliance control in the CFMMR differs in two very substantial ways. First, the modeling structure presented here is unique because the compliant frames encounter large deflections and may operate within post-buckled configurations during steering maneuvers. Therefore, it is difficult to model the compliant frame forces with great accuracy, although an approximate model of the compliant frame is developed based on the Finite Element Method (FEM) and the post-buckled frame element [5]. Second, flexible manipulators do not posses nonholonomic constraints, which are one of the typical characteristics of the CFMMR. Hence, the dynamic controllers developed for the CFMMR must consider nonlinear compliance effects and nonholonomic constraints typical of mobile robots, which prevent the application of traditional dynamic controllers for flexible manipulators. Compliance among mobile robots cooperatively manipulating an object has also received attention [15,16], but these efforts have focused on motion planning and coordination issues rather than robust dynamic motion control subject to nonholonomic constraints, which is the subject of this paper. The controller derived here could certainly benefit cooperative mobile robots, though.

In recent years, much attention has been paid to the motion control of mobile robots. Some research focuses only on the kinematic model (e.g. steering system) of a mobile robot where the input is velocity [3,17], and these can be called *kinematic motion controllers*. However, practically they need to take into account the specific dynamics that can produce the input velocity using wheel torque provided by the mobile robot. Thus, some research has been oriented toward torque-based control of dynamical models combined with kinematic models subject to nonholomomic constraints in order to improve tracking performance [18,19], which can be regarded as *dynamic motion control*. These efforts have focused only on rigid mobile robots not interacting cooperatively with other robots.

Control of the CFMMR requires that we consider compliant coupling (e.g., cooperation) between multiple axle modules. Thus,

Contributed by the Dynamic Systems, Measurement, and Control Division of ASME for publication in the JOURNAL OF DYNAMIC SYSTEMS, MEASUREMENT, AND CONTROL. Manuscript received December 14, 2004; final manuscript received January 13, 2006. Assoc. Editor: Sunil K. Agrawal.

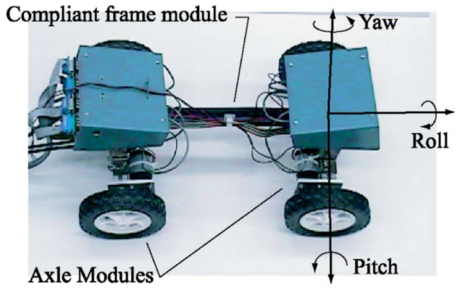

Fig. 1 Two-axle CFMMR experimental configuration

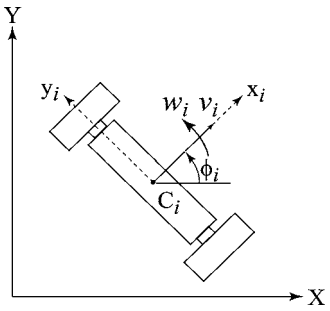

Fig. 2 The *i*th axle module kinematics

we use a curvature-based *kinematic motion controller* [3,4] to specify individual axle motion such that the CFMMR executes the desired net motion. These individual axle motions then provide real-time reference inputs to a *dynamic motion controller*. In our previous work, a perfect model of the CFMMR was assumed in the dynamic controller, which ultimately led to tracking error and necessary controller tuning for specific types of paths [5].

In reality, many kinds of disturbances always exist. Therefore, a few nonlinear, robust, and adaptive *dynamic motion control* techniques have been developed in the presence of the uncertainties of mobile robots [20–25] to confront the negative effects caused by approximation. Other researchers proposed discontinuous robust and/or adaptive controllers that complicate the adjustment of control gains to deal with instability caused by discontinuity, where the bounds of the uncertainties must be known [21–23]. Fierro proposed robust adaptive controllers using online neural networks. But a time-consuming computation is required, and it is difficult to guarantee the convergence of neural network controllers in real time [24,25]. Lin developed a robust damping control technique that does not require any knowledge of the bounds of the disturbances and had a fairly simple structure. Because of the complexity of the CFMMR dynamic model and the potentially large frame forces, the disturbances are unpredictable [20]. Hence, our robust controller is based on extension of [20]. Note that the reference velocities provided by our curvature-based *kinematic motion control* algorithms for posture regulation [3] and path following [4,26] are time varying, however, while constant reference velocities are assumed for simplicity in [20].

The major contribution of this work is development of model-based distributed robust control for the CFMMR, which is generally applicable to any cooperative mobile robotic system with uncertain compliant interaction forces. Two significant issues considered in the development of the controller are modeling and control of highly nonlinear interaction forces, which is novel, and dynamic tracking control of time-varying reference trajectories (velocity and posture specified as a function of time by a *kinematic motion controller*), which is an extension of previous work. As part of the major contribution, we experimentally validate the distributed robust controller performance with and without interaction force models and illustrate its capability to track time varying trajectories.

The structure of the paper follows. Modular kinematic and dynamic models of the CFMMR are derived in Sec. 2. A nonlinear damping controller for unicycle type robots with time varying reference velocities is proposed in Sec. 3. A distributed controller for general multi-module CFMMR configurations is proposed in Sec. 4. The distributed control algorithm is then applied to a two-axle CFMMR in simulation and experiment to evaluate their performance in Sec. 5. Concluding remarks and future work are described in Sec. 6.

2 Kinematic and Dynamic Models

2.1 Generic Modeling Structure. Consider the *i*th axle of an *n*-axle CFMMR, Fig. 2. Let us define a fixed global reference frame $F(X,Y)$ and moving frames $f_i(x_i,y_i)$ attached to the points C_i at the midpoint of the *i*th axle, where $i=1\ldots n$. At any instant, the *i*th axle module is rotating about the IC (Instantaneous Center), Fig. 3, such that the ICR's projections onto the x_i axes define point C_i at the midpoint of each axle. A module configuration vector $q_i=[X_i\ Y_i\ \phi_i]$ is then attached to this point and oriented with the axle. In order to describe this configuration within the context of the entire system, we assemble each of these module configuration vectors into a system configuration vector $Q=[q_1,\ldots,q_n]^T$ where $Q\in R^{3n\times 1}$. It is then possible to assemble a system description of the form,

$$\mathbf{M}(Q)\ddot{Q}+\mathbf{V}(Q,\dot{Q})\dot{Q}+\mathbf{F}(\dot{Q})+\mathbf{G}(Q)+\tau_d+\mathbf{F}_K(Q)=\mathbf{E}(Q)\tau-\mathbf{A}^T(Q)\lambda, \quad (1)$$

where $\mathbf{M}(Q)\in R^{3n\times 3n}$ is a symmetric, positive definite inertia matrix assembled from the individual axle module inertia matrices. Assembling individual axle module dynamic characteristics into the system model, $\mathbf{V}(Q,\dot{Q})\in R^{3n\times 3n}$ is the centripetal and coriolis forces, $\mathbf{F}(\dot{Q})\in R^{3n\times 1}$ denotes the friction, $\mathbf{G}(Q)\in R^{3n\times 1}$ is the gravitational vector, τ_d denotes bounded unknown disturbances including unstructured unmodeled dynamics, $\mathbf{E}(Q)\in R^{3n\times 2n}$ is the input transformation matrix, $\tau\in R^{2n\times 1}$ is the input torques, and $\lambda\in R^{n\times 1}$ is the vector of constraint forces. $\mathbf{A}(Q)\in R^{n\times 3n}$ is the global matrix associated with the nonholonomic constraints. Compliant frame forces are described by globally defined stiffness equations that are assembled into $\mathbf{F}_K(Q)\in R^{3n\times 1}$.

2.2 Modular Dynamic Models. First, the dynamic model of single-axle module is presented [18]. The generic matrices are then assembled assuming a serial configuration. Considering the *i*th axle module, we let $\mathbf{V}_i(q_i,\dot{q}_i)=\mathbf{0}$ since centripetal and coriolis

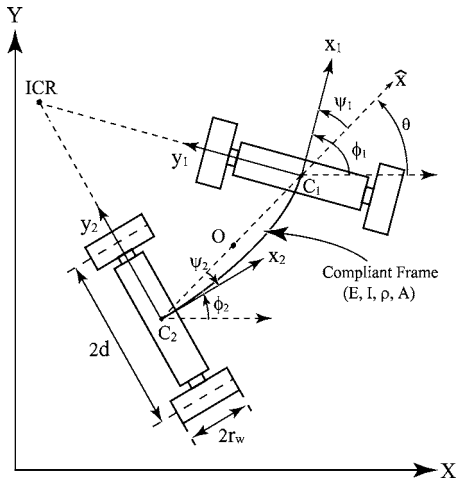

Fig. 3 General configuration of a two-axle CFMMR

forces of each axle are relatively small due to the velocity and curvature constraints of our robot. Also, $\mathbf{G}_i(q_i)=\mathbf{0}$ since motion of robot system is assumed to be in the horizontal plane. The mass matrix and the input transformation matrix of this axle module are:

$$\mathbf{M}_i(q_i)=\begin{bmatrix} m_i & 0 & 0 \\ 0 & m_i & 0 \\ 0 & 0 & J_i \end{bmatrix}, \quad \mathbf{E}_i(q_i)=\frac{1}{r_w}\begin{bmatrix} \cos\phi_i & \cos\phi_i \\ \sin\phi_i & \sin\phi_i \\ -d & d \end{bmatrix} \tag{2}$$

where m_i and J_i are mass and mass moment of the ith axle individually. The wheel torques applied to the ith axle module are denoted as $\tau_i=[\tau_{L,i}\ \tau_{R,i}]^T$, where $\tau_{L,i}$ and $\tau_{R,i}$ are motor torques acting on the left and right wheel, respectively. The corresponding frame reaction forces are then expressed as:

$$\mathbf{F}_{K,i}(q_i,q_j)=[F_{X,i}\ F_{Y,i}\ M_i]^T \tag{3}$$

where j denotes the numbers of all the axles connected with the ith axle, and the Lagrange multipliers are determined by,

$$\lambda_i=-m_i\dot{\phi}_i(\dot{X}_i\cos\phi_i+\dot{Y}_i\sin\phi_i)+F_{X,i}\sin\phi_i-F_{Y,i}\cos\phi_i \tag{4}$$

Therefore the ith axle dynamic equation is expressed as:

$$\mathbf{M}_i(q_i)\ddot{q}_i+\mathbf{F}(\dot{q}_i)+\tau_{d,i}+\mathbf{F}_{K,i}(q_i,q_j)=\mathbf{E}_i(q_i)\tau_i-\mathbf{A}_i^T(q_i)\lambda_i \tag{5}$$

Hence, the whole dynamic system is assembled by the above axle module matrices as:

$$\mathbf{M}(Q)=\begin{bmatrix} \mathbf{M}_1(q_1) & 0 & \cdots & 0 \\ 0 & \mathbf{M}_2(q_2) & 0 & \cdots \\ \cdots & 0 & \cdots & 0 \\ 0 & \cdots & 0 & \mathbf{M}_n(q_n) \end{bmatrix} \tag{6}$$

$$\mathbf{E}(Q)=\begin{bmatrix} \mathbf{E}_1(q_1) & 0 & \cdots & 0 \\ 0 & \mathbf{E}_2(q_2) & 0 & \cdots \\ \cdots & 0 & \cdots & 0 \\ 0 & \cdots & 0 & \mathbf{E}_n(q_n) \end{bmatrix} \tag{7}$$

$$\mathbf{F}_K(Q)=[\mathbf{F}_{K,1}\ \mathbf{F}_{K,2}\ \cdots\ \mathbf{F}_{K,n}]^T \tag{8}$$

$$\tau=[\tau_1\ \tau_2\ \cdots\ \tau_n]^T \tag{9}$$

2.3 Modular Kinematic Models. The kinematic model of the ith axle module is presented subject to nonholonomic constraints [18]. The generic kinematic matrices are then assembled similar to the dynamic matrices. Assuming pure rolling without slipping, the nonholonomic constraints of the ith axle module can be expressed in matrix form as

$$\mathbf{A}_i(q_i)\dot{q}_i=0 \tag{10}$$

where $\mathbf{A}_i(q_i)\in R^{1\times 3}$ is the matrix associated with the ith axle nonholonomic constraints:

$$\mathbf{A}_i(q_i)=[-\sin\phi_i\ \cos\phi_i\ 0] \tag{11}$$

Let $\mathbf{S}_i(q_i)\in R^{3\times 2}$ then be a full rank matrix formed by a set of smooth and linearly independent vector fields spanning the null space of $\mathbf{A}_i(q_i)$ such that

$$\mathbf{A}_i(q_i)\mathbf{S}_i(q_i)=\mathbf{0} \tag{12}$$

Equations (10) and (12) imply the existence of a two dimensional velocity vector $\mathbf{v}_i(t)\in R^{2\times 1}$ such that, for all time, t,

$$\dot{q}_i=\mathbf{S}_i(q_i)\mathbf{v}_i(t) \tag{13}$$

where

$$\mathbf{S}_i(q_i)=\begin{bmatrix} \cos\phi_i & 0 \\ \sin\phi_i & 0 \\ 0 & 1 \end{bmatrix} \tag{14}$$

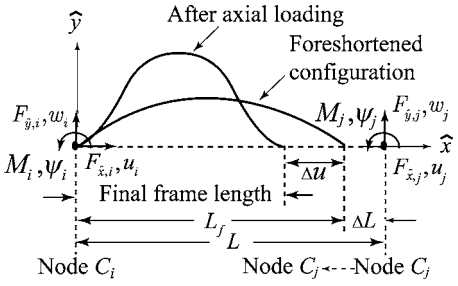

Fig. 4 The general configuration of single-finite-element of the compliant frame module

$$\mathbf{v}_i(t)=[v_i\ \omega_i]^T \tag{15}$$

and v_i and ω_i represent the linear and angular velocities of the ith axle at point C_i.

Likewise, the n-axle matrix associated with the nonholonomic for the serial configuration can be assembled as:

$$\mathbf{A}(Q)=\begin{bmatrix} \mathbf{A}_1(q_1) & \mathbf{0} & \cdots & \mathbf{0} \\ \mathbf{0} & \mathbf{A}_2(q_2) & \cdots & \vdots \\ \mathbf{0} & \mathbf{0} & \cdots & \mathbf{0} \\ \mathbf{0} & \cdots & \mathbf{0} & \mathbf{A}_n(q_n) \end{bmatrix} \tag{16}$$

There is also the existence of a $2n$ dimensional velocity vector $\mathbf{v}(t)\in R^{2n\times 1}$ such that, for all time, t,

$$\dot{Q}=\mathbf{S}(Q)\mathbf{v}(t) \tag{17}$$

where $\mathbf{S}(Q)\in R^{3n\times 2n}$ is a full rank matrix formed by a set of smooth and linearly independent vector fields spanning the null space of $\mathbf{A}(Q)$ such that

$$\mathbf{A}(Q)\mathbf{S}(Q)=\mathbf{0} \tag{18}$$

and $\mathbf{S}(Q)$ and $\mathbf{v}(t)$ can be assembled as

$$\mathbf{S}(Q)=\begin{bmatrix} \mathbf{S}_1(q_1) & \mathbf{0} & \cdots & \mathbf{0} \\ \mathbf{0} & \mathbf{S}_2(q_2) & \cdots & \vdots \\ \mathbf{0} & \mathbf{0} & \cdots & \mathbf{0} \\ \mathbf{0} & \cdots & \mathbf{0} & \mathbf{S}_n(q_n) \end{bmatrix} \tag{19}$$

$$\mathbf{v}(t)=[\mathbf{v}_1\ \mathbf{v}_2\ \cdots\ \mathbf{v}_n]^T \tag{20}$$

2.4 Compliant Frame Model. As we mentioned in Sec. 1, it is difficult to model the compliant frame forces with great accuracy. However, we can approximate the forces to improve controller performance. The behavior of the compliant frame element is complicated because of the interaction of the axle modules and the nonlinear frame behavior. To simplify matters, an approximate model of the compliant frame module is developed based on the Finite Element Method (FEM) and the post-buckled frame element [5,27]. The model includes the transverse and bending forces of a compliant beam, which will be used to develop the controller in the following sections.

Given L, E, and I as the free length, Young's Modulus, and area moment of inertia of the compliant frame, respectively, the frame model is expressed in the global coordinate frame with the local coordinate definition $w_i=w_j\equiv 0$, Fig. 4, as [28]

$$\mathbf{F}_K=\mathbf{R}^T\mathbf{K}\delta_L. \tag{21}$$

Here, $\mathbf{R}$ is a rotation transformation matrix with θ defined as in Fig. 3 such that,

$$\mathbf{R}=\begin{bmatrix}\mathbf{R}_\theta & \mathbf{0}\\ \mathbf{0} & \mathbf{R}_\theta\end{bmatrix} \text{ and } \mathbf{R}_\theta=\begin{bmatrix}\cos\theta & \sin\theta & 0\\ -\sin\theta & \cos\theta & 0\\ 0 & 0 & 1\end{bmatrix}. \quad (22)$$

For convenience, δ_L is measured relative to the ith node and described as a function of the axle configuration vectors to provide,

$$\delta_L=[0\ 0\ \psi_i\ -\Delta u\ 0\ \psi_j], \quad (23)$$

where the axial deflection caused by post-buckling, Δu, is defined as $L_f-[\hat{q}_j(1)-\hat{q}_i(1)]$ and the displacements $\hat{q}_c(1)$, $c=i,j$, can be calculated from the node locations C_i and C_j by using the axle configuration vectors, q_i and q_j, expressed in the local coordinate frame as,

$$[\hat{q}_c(1)\ \hat{q}_c(2)\ \psi_c]=\mathbf{R}_\theta q_c, \quad c=i,j \quad (24)$$

The foreshortened length L_f caused by bending moments is calculated as, [29]

$$L_f=L-\Delta L=L-\frac{2\psi_i^2-\psi_i\psi_j+2\psi_j^2}{30}L. \quad (25)$$

Note that for most cases, the compliant frame of the CFMMR is not straight due to steering maneuvers [3,29], and is essentially in a post-buckled shape. So the compliant frame is deflected by axial forces as well as bending moments. Therefore the relationship between the final frame length $\hat{q}_j(1)-\hat{q}_i(1)$ and the undeformed length L is expressed as $\hat{q}_j(1)-\hat{q}_i(1)=L-\Delta L-\Delta u$, Fig. 4.

For simplicity, we use a post-buckled axial stiffness that is linear and allows for a simple solution. The axial stiffness in post-buckling is modeled as $EI\pi^2/2L^3$ [5], which is much more compliant than the traditional rigid bar model used in frame elements. Therefore, $\mathbf{K}$ is obtained as the modified post-buckling stiffness matrix where,

$$\mathbf{K}=\begin{bmatrix}\mathbf{K}_{11} & \mathbf{K}_{12}\\ \mathbf{K}_{21} & \mathbf{K}_{22}\end{bmatrix}$$

$$\mathbf{K}_{11}=\frac{EI}{L^3}\begin{bmatrix}\pi^2/2 & 0 & 0\\ 0 & 12 & 6L\\ 0 & 6L & 4L^2\end{bmatrix}, \quad \mathbf{K}_{12}=\frac{EI}{L^3}\begin{bmatrix}-\pi^2/2 & 0 & 0\\ 0 & -12 & 6L\\ 0 & -6L & 4L^2\end{bmatrix}$$

$$\mathbf{K}_{21}=\mathbf{K}_{12}^T, \quad \mathbf{K}_{22}=\frac{EI}{L^3}\begin{bmatrix}\pi^2/2 & 0 & 0\\ 0 & 12 & -6L\\ 0 & -6L & 4L^2\end{bmatrix}. \quad (26)$$

3 Single Axle Nonlinear Damping Control Design

Due to the increased complexity of the system equations, the system is separated into two parts: (1) curvature-based *kinematic motion control*; and (2) robust *dynamic motion control*. Robust *dynamic motion control* is the main focus in this paper since the previously developed curvature-based *kinematic motion control* algorithms provide time-varying reference trajectories based on path state, s, and robot configuration [3,4,29]. These algorithms specify velocity trajectories for each axle to provide drift free curvature based steering algorithms for a two-axle CFMMR that minimize traction forces and account for frame foreshortening due to steering angles. Kinematic motion controllers for different configurations will be investigated in the future. The control system structure is presented in Fig. 5, which will be explained in the following subsections.

3.1 Structural Transformation of Single Axle Module. Considering the ith axle module, we rewrite the ith corresponding dynamic equation for the control design. Differentiating Eq. (13) with respect to time, substituting this result into Eq. (5), and then

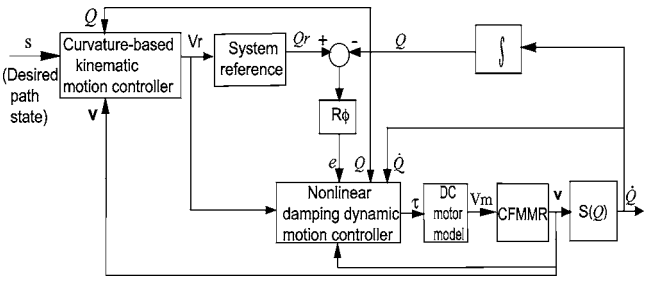

Fig. 5 A motion and dynamic control structure of the CFMMR

multiplying by $\mathbf{S}_i^{\mathbf{T}}(q_i)$, the constraint matrix $\mathbf{A}_i^T(q_i)\lambda_i$ can be eliminated. The ith axle dynamic equation of the CFMMR is then given by,

$$\mathbf{S}_i^T\mathbf{M}_i\mathbf{S}\dot{\mathbf{v}}_i+\mathbf{S}_i^T\mathbf{M}_i\dot{\mathbf{S}}\mathbf{v}_i+\mathbf{S}_i^T\mathbf{F}_i+\mathbf{S}_i^T\tau_{d,i}+\mathbf{S}_i^T\mathbf{F}_{K,i}(q_i,q_j)=\mathbf{S}_i^T\mathbf{E}_i\tau_i, \quad (27)$$

where Lagrange multipliers are no longer required and applied wheel torque is now an input to the system as a function of system states. Here we assume $\mathbf{F}_i=B_i\dot{q}_i$, where B_i consists of constant friction coefficients. The nonlinear part of the friction forces is included in $\tau_{d,i}$. Then rewrite Eq. (27) into the simplified form,

$$\bar{\mathbf{M}}_i\dot{\mathbf{v}}_i+\bar{B}_i\mathbf{v}_i+\bar{\tau}_{d,i}=\bar{\tau}_i, \quad (28)$$

where $\bar{\mathbf{M}}_i=\mathbf{S}_i^T\mathbf{M}_i\mathbf{S}_i$, $\bar{B}_i=\mathbf{S}_i^T(\mathbf{M}_i\dot{\mathbf{S}}_i+B_i\mathbf{S}_i)$, $\bar{\tau}_{d,i}=\mathbf{S}_i^T[\tau_{d,i}+\mathbf{F}_{K,i}(q_i,q_j)]$, $\bar{\tau}_i=\mathbf{S}_i^T\mathbf{E}_i\tau_i$.

The next step is to specify the dynamic extension of the velocity input, $\mathbf{v}_i\in R^{2\times 1}$, such that the regular backstepping form can be obtained:

$$\dot{q}_i=\mathbf{S}(q_i)\mathbf{v}_i \quad (29)$$

$$\bar{\mathbf{M}}_i\dot{\mathbf{v}}_i+\bar{B}_i\mathbf{v}_i+\bar{\tau}_{d,i}=\bar{\tau}_i. \quad (30)$$

These equations allow the two steering commands $\mathbf{v}_i(t)$ to be converted to desired wheel torques, $\tau_i(t)\in R^{2\times 1}$. The control objective is to derive a suitable $\tau_i(t)$ such that the CFMMR will track a specific smooth steering velocity $\mathbf{v}_{c,i}$ where,

$$\mathbf{v}_{c,i}(t)=[\nu_{c,i}\ \omega_{c,i}]^T. \quad (31)$$

This steering velocity as control input for the steering system (29) is chosen to achieve stable tracking of the reference trajectories, $q_{r,i}$. Then the CFMMR can achieve trajectory tracking given the derived wheel torques $\tau_i(t)$.

Since the reference velocity $\mathbf{v}_{r,i}$ is given by the previously mentioned motion controller, the reference trajectories $q_{r,i}$ can be solved from:

$$\dot{q}_{r,i}=S(q_{r,i})\mathbf{v}_{r,i} \quad (32)$$

Then the error state model for tracking is defined as,

$$e_i=\mathbf{R}_{\phi,i}(q_{r,i}-q_i), \quad (33)$$

where $q_{r,i}$ is the reference vector for the ith axle, $e_i\in R^{3\times 1}$ is the error position vector for the ith axle and,

$$e_i=[e_{X,i}\ e_{Y,i}\ e_{\phi,i}]^T. \quad (34)$$

As [30] shows, an alternative $\mathbf{v}_{c,i}$ is chosen as,

$$\mathbf{v}_{c,i}=\begin{bmatrix}\nu_{r,i}\cos e_{\phi,i}+k_{X,i}e_{X,i}\\ \omega_{r,i}+k_{Y,i}\nu_{r,i}e_{Y,i}+k_{\phi,i}\nu_{r,i}\sin e_{\phi,i}\end{bmatrix}, \quad (35)$$

where $k_{X,i},k_{Y,i},k_{\phi,i}$ are positive constants and $v_{r,i}$ are positive for the ith axle. The velocity control law $\mathbf{v}_{c,i}$ is thus proven [30] to make $e_i=0$ a stable equilibrium point using the Lyapunov function,

$$V_{1,i}(e_i) = \frac{1}{2}e_{X,i}^2 + \frac{1}{2}e_{Y,i}^2 + (1 - \cos e_{\phi,i})/k_{Y,i}, \tag{36}$$

and $V_{1,i}(e_i)$ is used in the subsequent controller development.

3.2 Properties and Assumptions of Single Axle Controller. There are several properties and assumptions that will be used in the following control design:

- *Assumption 1*: $\tau_{d,i}$ *and* $\mathbf{F}_{K,i}(q_i, q_j)$ *are bounded.*
- *Property 1*: $\|\bar{B}_i(q_i, \dot{q}_i)\| \leq b_i\|\dot{q}_i\| + c_i$, *where* b_i, c_i *are nonnegative constants.*
- *Property 2*: $\bar{\mathbf{M}}_i$ *is a constant matrix.*
- *Property 3*: $\dot{\mathbf{v}}_{c,i} = A_{1,i}\mathbf{v}_{c,i} + A_{2,i}\mathbf{v}_{r,i} + A_{3,i}\dot{\mathbf{v}}_{r,i}$, *where* $\|A_{1,i}\|$, $\|A_{2,i}\|$ *and* $\|A_{3,i}\|$ *are bounded.*

Proof: Properties 1 and 2 can be proven by a simple calculation, assuming the same mass of each module. Thus, we focus on the proof of Property 3.

Differentiating Eq. (35) yields,

$$\dot{\mathbf{v}}_{c,i} = \begin{bmatrix} k_{X,i}\dot{e}_{X,i} - \nu_{r,i}(\sin e_{\phi,i})\dot{e}_{\phi,i} + \dot{\nu}_{r,i}\cos e_{\phi,i} \\ \dot{\omega}_{r,i} + k_{Y,i}e_{Y,i}\dot{\nu}_{r,i} + k_{Y,i}\nu_{r,i}\dot{e}_{Y,i} + k_{\phi,i}\nu_{r,i}(\cos e_{\phi,i})\dot{e}_{\phi,i} + k_{\phi,i}\dot{\nu}_{r,i}\sin e_{\phi,i} \end{bmatrix} = \begin{bmatrix} k_{X,i} & 0 & -\nu_{r,i}(\sin e_{\phi,i}) \\ 0 & k_{Y,i}\nu_{r,i} & k_{\phi,i}\nu_{r,i}(\cos e_{\phi,i}) \end{bmatrix} \begin{bmatrix} \dot{e}_{X,i} \\ \dot{e}_{Y,i} \\ \dot{e}_{\phi,i} \end{bmatrix} + \begin{bmatrix} \cos e_{\phi,i} & 0 \\ k_{Y,i}e_{Y,i} + k_{\phi,i}\sin e_{\phi,i} & 1 \end{bmatrix} \begin{bmatrix} \dot{\nu}_{r,i} \\ \dot{\omega}_{r,i} \end{bmatrix}. \tag{37}$$

Substituting Eqs. (33) and (34) into Eq. (37) and applying Eq. (35), we can obtain,

$$\begin{aligned} \dot{\mathbf{v}}_{c,i} &= \begin{bmatrix} k_{X,i} & 0 & -\nu_{r,i}(\sin e_{\phi,i}) \\ 0 & k_{Y,i}\nu_{r,i} & k_{\phi,i}\nu_{r,i}(\cos e_{\phi,i}) \end{bmatrix} \begin{bmatrix} \omega_i e_{Y,i} - \nu_i + \nu_{r,i}\cos e_{\phi,i} \\ -\omega_i e_{X,i} + \nu_{r,i}\sin e_{\phi,i} \\ \omega_{r,i} - \omega_i \end{bmatrix} + \begin{bmatrix} \cos e_{\phi,i} & 0 \\ k_{Y,i}e_{Y,i} + k_{\phi,i}\sin e_{\phi,i} & 1 \end{bmatrix} \dot{\mathbf{v}}_{r,i} \\ &= \begin{bmatrix} -k_{X,i} & k_{X,i}e_{Y,i} + \nu_{r,i}\sin e_{\phi,i} \\ 0 & -k_{Y,i}\nu_{r,i}e_{X,i} - k_{\phi,i}\nu_{r,i}\cos e_{\phi,i} \end{bmatrix} \mathbf{v}_{c,i} + \begin{bmatrix} k_{X,i}\cos e_{\phi,i} & -\nu_{r,i}\sin e_{\phi,i} \\ k_{Y,i}\nu_{r,i}\sin e_{\phi,i} & k_{\phi,i}\nu_{r,i}\cos e_{\phi,i} \end{bmatrix} \mathbf{v}_{r,i} \\ &\quad + \begin{bmatrix} \cos e_{\phi,i} & 0 \\ k_{Y,i}e_{Y,i} + k_{\phi,i}\sin e_{\phi,i} & 1 \end{bmatrix} \dot{\mathbf{v}}_{r,i}. \end{aligned} \tag{38}$$

Finally, $\dot{\mathbf{v}}_{c,i}$ is simplified as,

$$\dot{\mathbf{v}}_{c,i} = A_{1,i}\mathbf{v}_{c,i} + A_{2,i}\mathbf{v}_{r,i} + A_{3,i}\dot{\mathbf{v}}_{r,i}, \tag{39}$$

where $A_{1,i}$, $A_{2,i}$, and $A_{3,i}$ are individually the coefficient matrix of $\mathbf{v}_{c,i}$, $\mathbf{v}_{r,i}$, and $\dot{\mathbf{v}}_{r,i}$.

Since $\|A_{1,i}\|$, $\|A_{2,i}\|$, and $\|A_{3,i}\|$ are checked to be bounded by inspection, Property 4 is proven. △

3.3 Nonlinear Damping Control Design of Single-Axle Module. We will now extend the nonlinear damping control scheme specified in [20] to a single-axle CFMMR configuration with time varying reference velocities.

Define the velocity error vector for each axle as,

$$\mathbf{e}_{c,i} = \begin{bmatrix} e_{\nu,i} \\ e_{\omega,i} \end{bmatrix} = \mathbf{v}_i - \mathbf{v}_{c,i} = \begin{bmatrix} \nu_i - \nu_{r,i}\cos e_{\phi,i} - k_{X,i}e_{X,i} \\ \omega_i - \omega_{r,i} - k_{Y,i}\nu_{r,i}e_{Y,i} - k_{\phi,i}\nu_{r,i}\sin e_{\phi,i} \end{bmatrix}. \tag{40}$$

Differentiating Eq. (40) and substituting Eq. (30) yields,

$$\bar{\mathbf{M}}_i\dot{\mathbf{e}}_{c,i} = \bar{\tau}_i - \bar{B}_i\mathbf{v}_i - \bar{\tau}_{d,i} - \bar{\mathbf{M}}_i\dot{\mathbf{v}}_{c,i}. \tag{41}$$

Then choose the Lyapunov candidate for the dynamic model, Eq. (30), as

$$V_{2,i}(\mathbf{e}_{c,i}) = \frac{1}{2}\mathbf{e}_{c,i}^T\bar{\mathbf{M}}_i\mathbf{e}_{c,i}. \tag{42}$$

Differentiating Eq. (42) yields:

$$\dot{V}_{2,i}(\mathbf{e}_{c,i}) = \mathbf{e}_{c,i}^T\bar{\mathbf{M}}_i\dot{\mathbf{e}}_{c,i} + \frac{1}{2}\mathbf{e}_{c,i}^T\dot{\bar{\mathbf{M}}}_i\mathbf{e}_{c,i}. \tag{43}$$

By substituting Eq. (41) into Eq. (43), we obtain,

$$\dot{V}_{2,i}(\mathbf{e}_{c,i}) = \mathbf{e}_{c,i}^T[\bar{\tau}_i - (\bar{B}_i\mathbf{v}_i + \bar{\mathbf{M}}_i\dot{\mathbf{v}}_{c,i} + \bar{\tau}_{d,i})] + \frac{1}{2}\mathbf{e}_{c,i}^T\dot{\bar{\mathbf{M}}}_i\mathbf{e}_{c,i}. \tag{44}$$

Applying Property 2 yields,

$$\dot{V}_{2,i}(\mathbf{e}_{c,i}) = \mathbf{e}_{c,i}^T[\bar{\tau}_i - (\bar{B}_i\mathbf{v}_i + \bar{\mathbf{M}}_i\dot{\mathbf{v}}_{c,i} + \bar{\tau}_{d,i})]. \tag{45}$$

Then applying Property 3 yields,

$$\dot{V}_{2,i}(\mathbf{e}_{c,i}) = \mathbf{e}_{c,i}^T[\bar{\tau}_i - (\bar{B}_i\mathbf{v}_i + \bar{\mathbf{M}}_iA_{1,i}\mathbf{v}_{c,i} + \bar{\mathbf{M}}_iA_{2,i}\mathbf{v}_{r,i} + \bar{\mathbf{M}}_iA_{3,i}\dot{\mathbf{v}}_{r,i} + \bar{\tau}_{d,i})]. \tag{46}$$

According to Properties 1, 3, and Assumption 1, we obtain,

$$\begin{aligned} \dot{V}_{2,i}(\mathbf{e}_{c,i}) &\leq \mathbf{e}_{c,i}^T\bar{\tau}_i + \|\mathbf{e}_{c,i}\|\{\|\bar{B}_i\|\,\|\mathbf{v}_i\| + \|\bar{\mathbf{M}}_i\|\,\|A_{1,i}\|\,\|\mathbf{v}_{c,i}\| \\ &\quad + \|\bar{\mathbf{M}}_i\|\,\|A_{2,i}\|\,\|\mathbf{v}_{r,i}\| + \|\bar{\mathbf{M}}_i\|\,\|A_{3,i}\|\,\|\dot{\mathbf{v}}_{r,i}\| + \|\bar{\tau}_{d,i}\|\} \leq \mathbf{e}_{c,i}^T\bar{\tau}_i \\ &\quad + \|\mathbf{e}_{c,i}\|\{b_i\|\mathbf{v}_i\|\,\|\mathbf{v}_i\| + c_i\|\mathbf{v}_i\| + \|\bar{\mathbf{M}}_i\|\,\|A_{1,i}\|\,\|\mathbf{v}_{c,i}\| \\ &\quad + \|\bar{\mathbf{M}}_i\|\,\|A_{2,i}\|\,\|\mathbf{v}_{r,i}\| + \|\bar{\mathbf{M}}_i\|\,\|A_{3,i}\|\,\|\dot{\mathbf{v}}_{r,i}\| + \|\tau_{d,i}\| \\ &\quad + \|\mathbf{F}_K(q_i, q_j)\|\} = \mathbf{e}_{c,i}^T\bar{\tau}_i + \|\mathbf{e}_{c,i}\|\delta_i^T\xi_i \end{aligned} \tag{47}$$

where,

$$\begin{aligned} \delta_i^T &= \{b_i, c_i, \|\bar{\mathbf{M}}_i\|\,\|A_{1,i}\|, \|\bar{\mathbf{M}}_i\|\,\|A_{2,i}\|, \|\bar{\mathbf{M}}_i\|\,\|A_{3,i}\|, \|\tau_{d,i}\|, 1\} \\ \xi_i^T &= \{\|\mathbf{v}_i\|\,\|\mathbf{v}_i\|, \|\mathbf{v}_i\|, \|\mathbf{v}_{c,i}\|, \|\mathbf{v}_{r,i}\|, \|\dot{\mathbf{v}}_{r,i}\|, 1, \|\mathbf{F}_{K,i}(q_i, q_j)\|\} \end{aligned} \tag{48}$$

Here δ_i is bounded by the above properties and assumptions, and ξ_i is a known, positive definite vector. Hence, in order to make Eq. (47) negative definite, choose,

$$\bar{\tau}_i = -K_i\mathbf{e}_{c,i}\|\xi_i\|^2, \tag{49}$$

where

$$K_i = \begin{bmatrix} K_{1,i} & 0 \\ 0 & K_{2,i} \end{bmatrix}$$

is the matrix control gain and $K_{1,i}$, $K_{2,i}$ are positive constants. The control input is then,

$$\tau_i = (\mathbf{S}_i^T \mathbf{E}_i)^{-1} \bar{\tau}_i = -(\mathbf{S}_i^T \mathbf{E}_i)^{-1} K_i \mathbf{e}_{c,i} \|\xi_i\|^2. \tag{50}$$

Substitute Eq. (49) into Eq. (47),

$$\begin{aligned} \dot{V}_{2,i}(\mathbf{e}_{c,i}) &= -\mathbf{e}_{c,i}^T K_i \mathbf{e}_{c,i} \|\xi_i\|^2 + \|\mathbf{e}_{c,i}\| \delta_i^T \xi_i \\ &\leqslant -\|K_i\| \|\mathbf{e}_{c,i}\|^2 \|\xi_i\|^2 + \|\mathbf{e}_{c,i}\| \|\delta_i\| \|\xi_i\| \\ &= -\|K_i\| \left\{ \|\mathbf{e}_{c,i}\| \|\xi_i\| - \frac{\|\delta_i\|}{2\|K_i\|} \right\}^2 + \frac{\|\delta_i\|^2}{4\|K_i\|} \end{aligned} \tag{51}$$

By using the Lyapunov function $V_i = V_{1,i} + V_{2,i}$ [20,31], $\mathbb{C}_i = [\mathbf{e}_i \ \mathbf{e}_{c,i}]^T$ is globally uniformly bounded and the velocity tracking error becomes arbitrarily small by increasing the control gain K_i.

Note that the reference velocity vector is included in the control input since the motion controller could provide time varying reference velocities. The compliant frame force $\mathbf{F}_{K,i}(q_i, q_j)$ is also taken consideration in the controller, which is the topic of the next subsection.

3.4 Compliant Frame Effect on Control Design. There are two cases to consider for the CFMMR in terms of the compliant frame effect on control design. On one hand, the approximate model of the compliant frame force, $\mathbf{F}_{K,i}(q_i, q_j)$, may be used and the inaccurate part of this model will become part of the disturbance, $\tau_{d,i}$, and δ_i and ξ_i are chosen per Eq. (48). On the other hand, $\mathbf{F}_{K,i}(q_i, q_j)$ may be considered to be totally unknown and δ_i and ξ_i will be redefined as

$$\delta_i^T = \{b_i, c_i, \|\bar{\mathbf{M}}_i\| \|A_{1,i}\|, \|\bar{\mathbf{M}}_i\| \|A_{2,i}\|, \|\bar{\mathbf{M}}_i\| \|A_{3,i}\|, \|\tau_{d,i} + \mathbf{F}_{K,i}(q_i, q_j)\|\}$$

$$\xi_i^T = \{\|\mathbf{v}_i\| \|\mathbf{v}_i\|, \|\mathbf{v}_i\|, \|\mathbf{v}_{c,i}\|, \|\mathbf{v}_{r,i}\|, \|\dot{\mathbf{v}}_{r,i}\|, 1\} \tag{52}$$

which helps to decrease computational requirements since $\mathbf{F}_{K,i}(q_i, q_j)$ is not calculated between time steps.

We will apply both control inputs determined by Eqs. (48) and (52) to the experimental platform and compare them in Sec. 5 in order to determine the characteristics of performance, tracking errors, and computations.

4 Multi-axle Distributed Control Design

The distributed controller is designed for a multiaxle CFMMR based on the above single-axle controller. That is to say, the distributed controller is composed of n independent controllers $\tau_j, j = 1 \sim n$ as:

$$\tau_j = -(\mathbf{S}_j^T \mathbf{E}_j)^{-1} K_j \mathbf{e}_{c,j} \|\xi_j\|^2. \tag{53}$$

Proposition: The multiaxle CFMMR can achieve stable trajectory tracking with the distributed controller (53) *if the response of each module is globally uniformly bounded by its corresponding single-axle controller.*

Proof: Choose the composite Lyapunov function candidate,

$$\begin{aligned} V = V_1 + \ \dots \ + V_i + \ \dots \ + V_n = V_{1,1} + V_{2,1} + \ \dots \ + V_{1,i} + V_{2,i} + \ \dots \\ + V_{1,n} + V_{2,n}. \end{aligned} \tag{54}$$

Substituting Eqs. (36) and (42) into Eq. (54) produces,

$$\begin{aligned} V = \frac{1}{2} e_{X,1}^2 + \frac{1}{2} e_{Y,1}^2 + (1 - \cos e_{\phi,1})/k_{Y,1} + \frac{1}{2} \mathbf{e}_{c,1}^T \bar{\mathbf{M}}_1 \mathbf{e}_{c,1} + \ \dots \ + \frac{1}{2} e_{X,i}^2 \\ + \frac{1}{2} e_{Y,i}^2 + (1 - \cos e_{\phi,i})/k_{Y,i} + \frac{1}{2} \mathbf{e}_{c,i}^T \bar{\mathbf{M}}_i \mathbf{e}_{c,i} + \ \dots \ + \frac{1}{2} e_{X,n}^2 + \frac{1}{2} e_{Y,n}^2 \\ + (1 - \cos e_{\phi,n})/k_{Y,n} + \frac{1}{2} \mathbf{e}_{c,n}^T \bar{\mathbf{M}}_n \mathbf{e}_{c,n}. \end{aligned} \tag{55}$$

Differentiating Eq. (55) and applying Eqs. (33) and (51) yields,

$$\begin{aligned} \dot{V} \leqslant & -k_{X,1} e_{X,1}^2 - \frac{k_{\phi,1}}{k_{Y,1}} \nu_{r,1} \sin^2 e_{\phi,1} - \|K_1\| \left\{ \|\mathbf{e}_{c,1}\| \|\xi_1\| - \frac{\|\delta_1\|}{2\|K_1\|} \right\}^2 \\ & + \frac{\|\delta_1\|^2}{4\|K_1\|} - \ \dots \ - k_{X,i} e_{X,i}^2 - \frac{k_{\phi,i}}{k_{Y,i}} \nu_{r,i} \sin^2 e_{\phi,i} - \|K_i\| \left\{ \|\mathbf{e}_{c,i}\| \|\xi_i\| \right. \\ & \left. - \frac{\|\delta_i\|}{2\|K_i\|} \right\}^2 + \frac{\|\delta_i\|^2}{4\|K_i\|} - \ \dots \ - k_{X,n} e_{X,n}^2 - \frac{k_{\phi,n}}{k_{Y,n}} \nu_{r,n} \sin^2 e_{\phi,n} - \|K_n\| \\ & \times \left\{ \|\mathbf{e}_{c,n}\| \|\xi_n\| - \frac{\|\delta_n\|}{2\|K_n\|} \right\}^2 + \frac{\|\delta_n\|^2}{4\|K_n\|}, \end{aligned} \tag{56}$$

where $K_1, \dots, K_n$ are positive definite matrices, $k_{X,1}, \dots, k_{X,n}, k_{Y,1}, \dots, k_{Y,n}, k_{\phi,1}, \dots, k_{\phi,n}$ are positive constants, and $\|\delta_1\|, \dots, \|\delta_n\|$ are bounded. Therefore,

$$\begin{aligned} \dot{V} \leqslant & -k_{X,1} e_{X,1}^2 - \frac{k_{\phi,1}}{k_{Y,1}} \nu_{r,1} \sin^2 e_{\phi,1} - \ \dots \ - k_{X,i} e_{X,i}^2 - \frac{k_{\phi,i}}{k_{Y,i}} \nu_{r,i} \sin^2 e_{\phi,i} \\ & - \ \dots \ - k_{X,n} e_{X,n}^2 - \frac{k_{\phi,n}}{k_{Y,n}} \nu_{r,n} \sin^2 e_{\phi,n} \\ = & -W(\mathbf{e}), \end{aligned} \tag{57}$$

when,

$$\|\mathbf{e}_{c,1}\| \geqslant \frac{1}{\|K_1\|} \frac{\|\delta_1\|}{\|\xi_1\|}, \dots, \|\mathbf{e}_{c,n}\| \geqslant \frac{1}{\|K_n\|} \frac{\|\delta_n\|}{\|\xi_n\|}, \tag{58}$$

where $\mathbf{e} = [\mathbb{C}_1 \ \dots \ \mathbb{C}_n]^T$, $\mathbb{C}_j = [\mathbf{e}_j \ \mathbf{e}_{c,j}]^T$, $j = 1 \sim n$, and $W(\mathbf{e})$ is a continuous positive definite function.

Hence we conclude that $\mathbf{e}$ is globally uniformly bounded [31]. According to Eq. (58), the tracking error bounds of each module becomes smaller as the norm of the corresponding control gain matrix, K_i, is increased. However, tracking error bound for the multiaxle CFMMR becomes more complicated. The modules are interconnected by compliant frames, so the behavior of each module can affect the others. Increasing the control gain for one axle may increase the tracking error of another. Second, the tracking error bounds are increased as the term δ_i increases, which may be caused by increased disturbances or model uncertainty. Therefore it is proper to minimize the tracking errors for the entire system by experimentally tuning the set of control gains, $K_1, \dots, K_n$. Δ

5 Controller Evaluation

5.1 Methods and Procedures. The distributed nonlinear damping controller for the two-axle CFMMR was simulated in MATLAB® and SIMULINK®. The reference velocities $\mathbf{v}_r$ of both axles are generated by a drift-free curvature-based *kinematic motion control* algorithm guiding midpoint, O, of the robot to follow the desired path [4,26]. The velocity trajectories are specified for each axle such that the distance between points C_1 and C_2 remains consistent with the ideal foreshortened length, L_f, of the frame given the current axle headings [29]. As we mentioned in Sec. 4, the control gains need to be tuned to minimize the tracking error bounds. The gains were first tuned in simulation until the tracking errors were within 10^{-3} with a similar time step size, 10^{-3}. These gains were then verified in experiment.

Several experiments were conducted on a two-module CFMMR

Table 1 Prototype of a two-module CFMMR

Parameter	Value	Units	Description
r_w	0.073	Meters	Wheel radius
d	0.162	Meters	Axle width (half)
m_i	4.76	Kg	Mass of each axle
J_i	0.0186	Kg/m^2	Mass moment of inertia of each axle

Table 2 Parameters of compliant frame

Parameter	Value	Units	Descriptions
L	0.37	meters	Length
w	0.05	meters	Width
t	0.7	mm	Thickness
E	2.0×10^{11}	Pa	Young's modulus
A	3.5×10^{-5}	m^2	Cross-sectional area
ρ	7.8×10^{3}	Kg/m^3	Density
I	1.4292×10^{-12}	m^4	Area moment of inertia

Table 3 Initial positions of three different shapes.

Path	x	y	ϕ
Line	−0.1	0.1	0
Circle	1.05	−0.2	$\pi/2$
Sine wave	−0.09	−0.04	$\pi/4$

experimental platform, Fig. 1, at the University of Utah. The robot is controlled via tether by a dSpace™ 1103 DSP board and an external power supply. Each wheel is actuated by a geared dc motor with voltage input V_m, Fig. 5. The real-time position of each wheel is detected by an encoder and odometry is used for predicting the axle posture. Video is used to illustrate the robot performance. Here we apply controllers with and without beam force compensation to consider their effect on performance.

The prototype parameters, Table 1, and the parameters of the compliant frame, Table 2, are used for both simulations and experiments. Three different path shapes, a straight line, a circle, and a sine wave were used with nonzero initial positions of midpoint O, Table 3. The straight line is the simplest path, where the reference is only a constant linear velocity. The circle is more complicated since the reference is ultimately constant linear and angular velocities. The sine wave is the most complicated, since the path consists of time varying linear and angular velocities. Therefore, the tracking performance of the robot can be evaluated comprehensively.

5.2 Results. Using the tuned gains

$$K_1 = K_2 = \begin{bmatrix} 30 & 0 \\ 0 & 5 \end{bmatrix},$$

the simulation results predict that the robot follows the corresponding desired paths perfectly. Experimental odometry results corroborate the simulated results well, except for some chattering and apparent wheel slippage.

Figure 6 shows the experimental posture data (according to

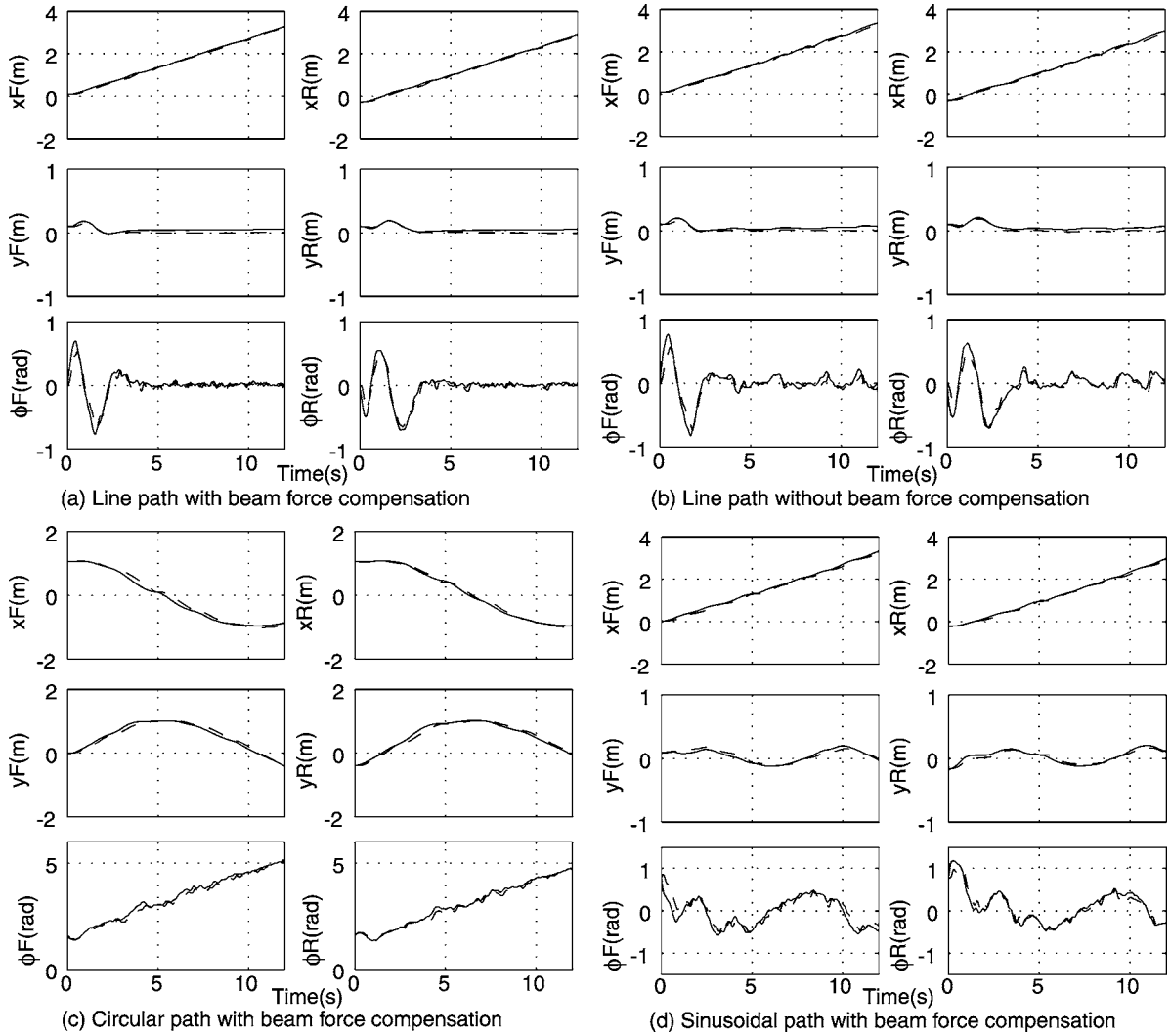

Fig. 6 Experimental posture data for path following, where solid lines represent the desired position and dashed lines represent the experimentally determined position

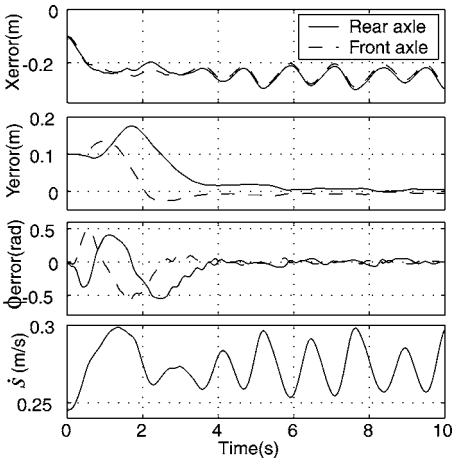

Fig. 7 Experimental position errors of each axle and reference velocity of middle point *O* while line path following according to odometric data

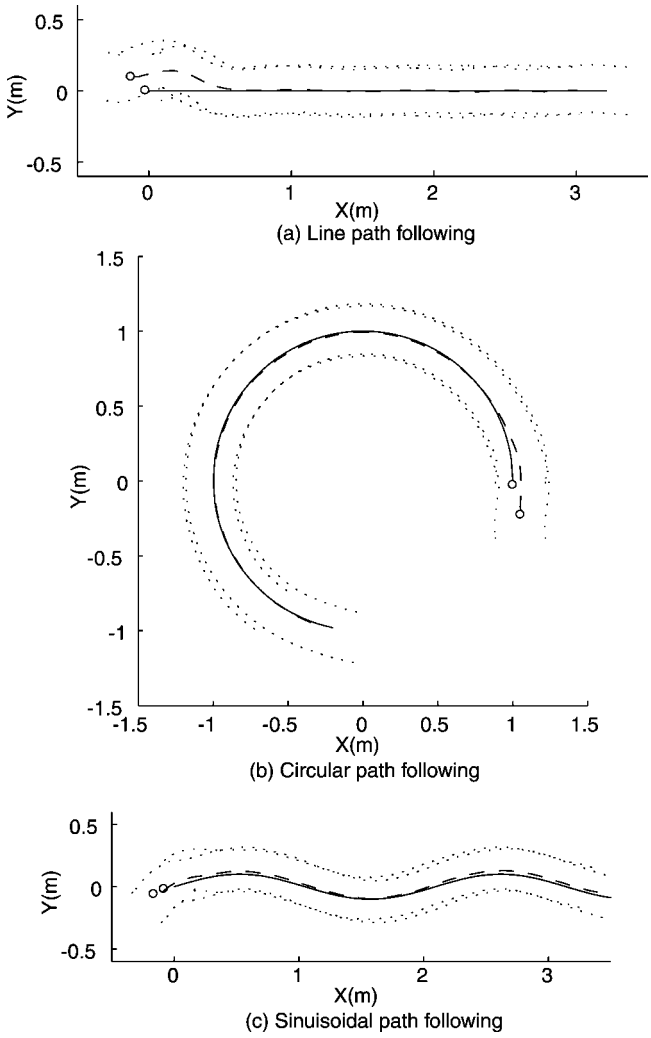

Fig. 8 Experimental path following results without beam force compensation according to odometric data

odometry) of the path following both with and without beam force compensation. The desired position is represented by the solid lines and the experimentally determined position is represented by the dashed lines. Figure 7 shows the position errors of each axle and the reference velocity, $\dot{s}$, of the midpoint O, where the position error of the rear axle is represented by the solid line and the position error of the front axle is represented by the dashed line. Figure 8 shows the experimental path following results without beam force compensation, where the desired trajectory of the midpoint, O, of the robot is represented by the solid line, the experimental trajectory of the midpoint, O, is represented by the dashed line, and the trajectory of the wheels are represented by dotted lines. Figure 9 shows the snapshots of the video for the line path following. The dotted lines are from simulation results, which represent the path of the midpoint O and each wheel, respectively. The white line illustrates the actual path that the robot converges to, which is parallel to the desired path (along the x axis), but offset by −0.06 m. Note that according to odometry, however, the robot converges to the specified paths quite well, Fig. 6. All of these results were conducted with the robot on a smooth, flat, high traction carpet surface.

5.3 Discussion. As Fig. 6 indicates, the system performed well while following the paths; even with nonzero initial error states and uncertain disturbance due to model inaccuracy. Note that compared with the pure model-based backstepping controller presented in [5], the nonlinear damping controller derived here compensates model uncertainty and does not need to adjust the control gains during the experiments. Thus, once the control gains are tuned properly in simulation, they can be used in experiment directly without off-tracking, as witnessed in previous results. This critical characteristic demonstrates the robustness of the controller applied to groups of axle modules bound by uncertain interaction forces.

As Figs. 6(*a*) and 6(*b*) indicate, while the line path following the controller with beam force compensation can achieve tighter performance and less tracking error, but more computation is required to predict those forces. The controller without beam force compensation is less aggressive at the cost of increasing the tracking error slightly. Both of them work well with the two-axle CFMMR. However, as the configuration and the environment become more and more complicated, the compliant frame forces will play more important roles in the robot performance. The controller with beam force compensation will be preferable, even though more computation will be required. Therefore, in the near future, the controller with beam force compensation will be used for the two-axle CFMMR on the rough terrain, such as on sand or with scattered rocks. Additional relative position sensors will then be introduced to help measure the relative position between the adjacent modules and predict the compliant frame forces more accurately.

As Fig. 7 indicates, the actual X position lags the reference position and oscillates. The Y position errors converge to a small value close to zero. The ϕ errors converge well except for a small chattering. Note that the reference velocity, $\dot{s}$, of the middle point O has oscillations that causes the oscillation of X position errors. These oscillations also cause, in part, the saturation of the wheel torques, Fig. 10, which will be discussed later. In the design of curvature-based *kinematic motion controller*, a positive constant ε was introduced to make this controller smooth. This introduction of ε causes the lagged X position, however. Improving the *kinematic motion control* to solve the lag problem is a subject of future work.

The 0.06 m-odometry error is observed in Fig. 9, which is mainly caused by wheel slippage. The apparent wheel slippage occurred in the first second because of the fast maneuvering turn of the robot. The torque saturation was also observed in the experiments, see Figs. 10(*d*). First, the saturation is caused by phase lag in the odometry measurement system. In the odometry system, second-order filters are used to decrease measurement noise. The filter also increases phase lag and makes the system closer to marginal stability. In this case, the filter was chosen to reduce the

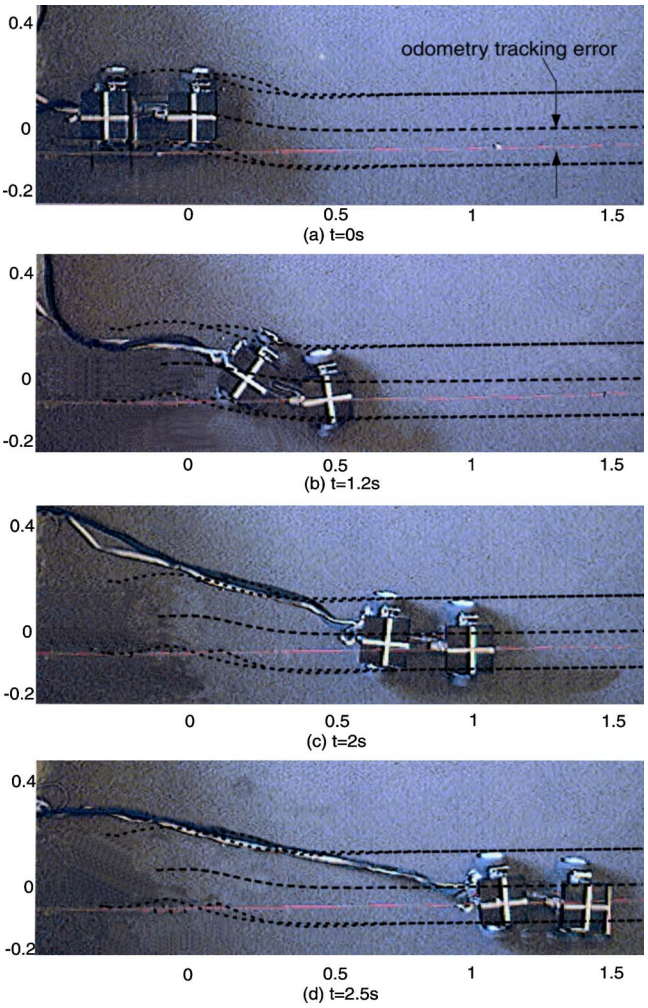

Fig. 9 Snapshots of line path following without beam compensation

noise, but introduced the corresponding oscillations and aggravated saturation. Additional sensor fusion algorithms will be used to reduce the odometry problems in the near future.

As Fig. 10 indicates, unmodeled uncertainties of the robot also contribute to torque saturation. In order to evaluate this problem, a series of line path following experiments were performed on surfaces with increasing traction characteristics, such as no ground contact, on sand, and on carpet. In the case of no ground contact, the robot was put on a box so that all the wheels are free to rotate without any surface interaction. It was used to narrow down the possible causes of torque saturation. Figure 10(*a*) shows the simulation results of the wheel torques. Figures 10(*b*)–10(*d*) show the experimental results in the three mentioned conditions. The average percent saturation for all the wheels in each case is investigated as well, Table 4. As Fig. 10 and Table 4 show, (*b*)–(*d*) have saturation that does not appear in simulation, which predicts that the unmodeled plant characteristics (such as backlash, unmodeled frame forces, friction, etc.) cause the saturation. Comparing (*c*) and (*d*) with (*b*), note that (*b*) has the least uncertainties caused by

Table 4 Analysis data of average torque saturation

Condition	In simulation	No ground contact	On sand	On carpet
Saturation percentage	0	19	28	32

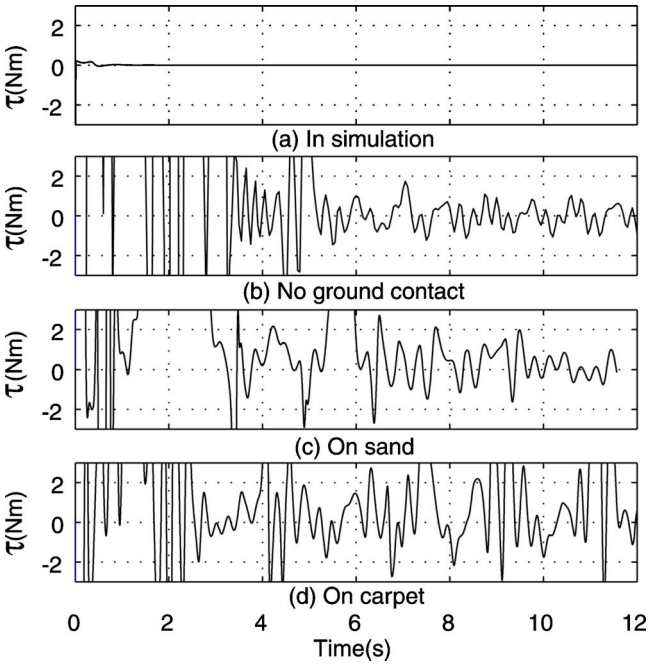

Fig. 10 Experimental and simulation results illustrating torque saturation of the front left wheel while line path following

the flexible frame and friction, and, therefore, has the least saturation. Comparing (*b*) and (*c*) with (*d*), note that (*d*) has the highest traction on carpet, and therefore has the most saturation. Hence, the torque saturation increases as the number of uncertainties of the robot increases. Hence, it is concluded that torque saturation is caused, in part, by model uncertainty.

6 Conclusions

In this paper we introduce a distributed nonlinear damping controller for dynamic motion control of wheeled Compliant Framed Modular Mobile Robots to compensate for model uncertainty with unknown bounds. Simulation and experimental results for a two-axle CFMMR configuration demonstrate the robustness of the proposed controller. This control algorithm is generally applicable to other mobile robots, which have unknown or partially known uncertainties. Future work will focus on improving the kinematic motion control, additional sensor algorithms incorporating relative position sensors, and the behavior of the CFMMR on the rough terrain.

Acknowledgment

The authors gratefully acknowledge support of this research provided by NSF Grant No. IIS-0308056.

References

[1] Yim, M., Roufas, K., Duff, D., Zhang, Y., Eldershaw, C., and Homans, S., 2003, "Modular Reconfigurable Robots in Space Applications," Auton. Rob., **14**, pp. 225–237.
[2] Ambrose, R. O., Aalund, M. P., and Tesar, D., 1993, "Designing Modular Robots for a Spectrum of Space Applications," in *Cooperative Intelligent Robotics in Space III*, 16–18 Nov 1992, Boston, MA, pp. 371–381.
[3] Albiston, B. W., and Minor, M. A., 2003, "Curvature Based Point Stabilization for Compliant Framed Wheeled Modular Mobile Robots," in *IEEE ICRA*, 14–19 Sep 2003, Taipei, Taiwan, pp. 83–89.
[4] Albiston, B. W., 2003, "Curvature Based Point Stabilization and Path Following for Compliant Framed Wheeled Modular Mobile Robots," Masters Thesis, University of Utah, Salt Lake City, UT, 92 pp.
[5] Park, S., and Minor, M. A., 2004, "Modeling and Dynamic Control of Compliant Framed Wheeled Modular Mobile Robots," in *IEEE ICRA*, Apr 26–May 1 2004, New Orleans, LA, pp. 3937–3943.
[6] Merrell, R., and Minor, M. A., 2003, "Internal Posture Sensing for a Flexible Frame Modular Mobile Robot," in *IEEE ICRA*, 14–19 Sep 2003, Taipei, Tai-

wan, pp. 452–457.
[7] Bekker, M. G., 1962, "Vehicle With Flexible Frame," U.S. Patent 3235020.
[8] Borenstein, J., 1995, "Control and Kinematic Design of Multi-Degree-of-Freedom Mobile Robots With Compliant Linkage," IEEE Trans. Rob. Autom., **11**, pp. 21–35.
[9] Mori, M., and Hirose, S., 2002, "Three-Dimensional Serpentine Motion and Lateral Rolling by Active Cord Mechanism ACM-R3," in *Proc. 2002 IEEE/RSJ Int'l Conf. Intel. Rob. and Sys. (IROS '02)*, 30 Sep–4 Oct, Lausanne, Switzerland, pp. 829–834.
[10] Kamegawa, T., Yamasaki, T., Igarashi, H., and Matsuno, F., 2004, "Development of the Snake-Like Rescue Robot KOHGA," in *Proc. 2004 IEEE Int'l Conf. on Rob. and Autom.*, 26 Apr–1 May, New Orleans, LA, pp. 5081–5086.
[11] Klaassen, B., and Paap, K. L., 1999, "GMD-SNAKE2: A Snake-Like Robot Driven by Wheels and a Method for Motion Control," *Proc. 1999 IEEE Int'l Conf. on Rob. and Autom., ICRA99*, Detroit, MI, 10–15 May, Vol. 4, pp. 3014–3019.
[12] Kimura, H., and Hirose, S., 2002, "Development of Genbu: Active Wheel Passive Joint Articulated Mobile Robot," in *2002 IEEE/RSJ Int'l Conf. on Intel. Rob. and Sys.(IROS 02)*, 30 Sep–4 Oct, Lausanne, Switzerland, pp. 823–828.
[13] Cheong, J., Chung, W. K., and Youm, Y., 2002, "PID Composite Controller and its Tuning for Flexible Link Robots," in *IEEE/RSJ Int. Conf. on Intelligent Robots and Systems*, 30 Sep–4 Oct 2002, Lausanne, Switzerland, pp. 2122–2127.
[14] Wang, X., and Mills, J. K., 2004, "A FEM Model for Active Vibration Control of Flexible Linkages," in *Proc.-IEEE ICRA*, 26 Apr–1 May 2004, New Orleans, LA, pp. 4308–4313.
[15] Hirata, Y., Kume, Y., Sawada, T., Wang, Z.-D., and Kosuge, K., 2004, "Handling of an Object by Multiple Mobile Manipulators in Coordination Based on Caster-Like Dynamics," in *2004 IEEE ICRA*, 26 Apr–1 May 2004, New Orleans, LA, pp. 807–812.
[16] Tang, C. P., Bhatt, R., and Krovi, V., 2004, "Decentralized Kinematic Control of Payload Transport by a System of Mobile Manipulators," in *2004 IEEE ICRA*, 26 Apr–1 May 2004, New Orleans, LA, pp. 2462–2467.
[17] Tayebi, A., Tadjine, M., and Rachid, A., 1997, "Invariant Manifold Approach for the Stabilization of Nonholonomic Systems in Chained Form: Application to a Car-Like Mobile Robot," in *Proc. of the 1997 36th IEEE Conf. on Decision and Control*, Part 4 (of 5), 10–12 December 1997, San Diego, CA, pp. 4038–4043.
[18] Fierro, R., and Lewis, F. L., 1997, "Control of a Nonholonomic Mobile Robot: Backstepping Kinematics Into Dynamics," J. Rob. Syst., **14**, pp. 149–163.
[19] Yang, J.-M., and Kim, J.-H., 1999, "Sliding Mode Motion Control of Nonholonomic Mobile Robots," IEEE Trans. Control Syst. Technol., **19**, pp. 15–23.
[20] Lin, S., and Goldenberg, A., 2000, "Robust Damping Control of Wheeled Mobile Robots," in *ICRA 2000*, 24–28 Apr 2000, San Francisco, CA, pp. 2919–2924.
[21] Wang, Z. P., Ge, S. S., and Lee, T. H., 2004, "Robust Motion/Force Control of Uncertain Holonomic/Nonholonomic Mechanical Systems," *IEEE/ASME Transactions on Mechatronics*, **9**, pp. 118–123.
[22] Wilson, D. G., and Robinett, III, R. D., 2001, "Robust Adaptive Backstepping Control for a Nonholonomic Mobile Robot," in *IEEE Int. Conf. on Systems, Man and Cybernetics*, 7–10 Oct 2001, Tucson, AZ, pp. 3241–3245.
[23] Kim, M. S., Shin, J. H., and Lee, J. J., 2000, "Design of a Robust Adaptive Controller for a Mobile Robot," in *IEEE/RSJ International Conference on Intelligent Robots and Systems*, 31 Oct–5 Nov 2000, Takamatsu, pp. 1816–1820.
[24] Fierro, R., and Lewis, F. L., 1998, "Control of a Nonholonomic Mobile Robot Using Neural Networks," IEEE Trans. Neural Netw., **9**, pp. 589–600.
[25] Fierro, R., and Lewis, F. L., 1996, "Practical Point Stabilization of a Nonholonomic Mobile Robot Using Neural Networks," in *Proceedings of the 1996 35th IEEE Conference on Decision and Control*, 11–13 Dec 1996, Kobe, Japan, pp. 1722–1727.
[26] Tayebi, A., and Rachid, A., 1997, "A Unified Discontinuous State Feedback Controller for the Path-Following and the Point-Stabilization Problems of a Unicycle-Like Mobile Robot," in *Proc. of the 1997 IEEE Int. Conf. on Control Applications*, Hartford, CT, pp. 31–35.
[27] Park, S., 2004, "Modeling and Dynamic Control for Compliant Framed Wheeled Modular Mobile Robots," in *Mechanical Engineering*, Salt Lake City, University of Utah.
[28] Spanski, P. L., 1970, "Flexible Frame Vehicle," U.S. Patent 3550710.
[29] Minor, M. A., Albiston, B., and Schwensen, C., 2006, "Simplified Motion Control of a Two-Axle Compliant Framed Wheeled Mobile Robot," IEEE Trans. Rob. Autom., **22**, pp. 491–506.
[30] Kanayama, Y., Kimura, Y., Miyazaki, F., and Noguchi, T., 1990, "A Stable Tracking Control Method for an Autonomous Mobile Robot," in *1990 IEEE ICRA*, 13–18 May 1990, Cincinnati, OH, pp. 384–389.
[31] Khalil, H., 2002, *Nonlinear Systems*, 3rd ed., Prentice–Hall, Upper Saddle River, NJ.